

Inclusive diffraction at the LHeC and FCC-eh

Néstor Armesto¹, Paul R. Newman², Wojciech Słomiński³, and Anna M. Staśto⁴

¹*Instituto Galego de Física de Altas Enerxías IGFAE, Universidade de Santiago de Compostela, 15782 Santiago de Compostela, Galicia-Spain*

²*School of Physics and Astronomy, University of Birmingham, UK*

³*Institute of Physics, Jagiellonian University, Krakow, Poland*

⁴*Department of Physics, Penn State University, University Park, PA 16802, USA*

December 15, 2024

Abstract

We analyse the possibilities for the study of inclusive diffraction offered by future electron–proton/nucleus colliders in the TeV regime, the Large Hadron-electron Collider as an upgrade of the HL-LHC and the Future Circular Collider in electron-hadron mode. Compared to ep collisions at HERA, we find an extension of the available kinematic range in x by a factor of order 20 and of the maximum Q^2 by a factor of order 100 for LHeC, while the FCC version would extend the coverage by a further order of magnitude both in x and Q^2 . This translates into a range of available momentum fraction of the diffractive exchange with respect to the hadron (ξ), down to $10^{-4} - 10^{-5}$ for a wide range of the momentum fraction of the parton with respect to the diffractive exchange (β). Using the same framework and methodology employed in previous studies at HERA and under very conservative assumptions for the luminosities and systematic errors, we find an improvement in the extraction of diffractive parton densities from fits to reduced cross sections for inclusive coherent diffraction in ep by about an order of magnitude. We analyse the sensitivity to kinematic cuts and variations of the fit framework. We also note sensitivity to the shape of the gluon distribution, and to physics beyond linear twist-2 DGLAP evolution at moderate Q^2 . For eA , we find that an extraction of the currently unmeasured nuclear diffractive parton densities is possible with similar accuracy to that in ep .

1 Introduction

Deep Inelastic Scattering (DIS) of a lepton on a proton is the cleanest way to explore the proton structure. The HERA accelerator at Hamburg was the only ep collider to date. It scattered electrons and positrons on protons, at centre-of-mass energy $\sqrt{s} = 318 \text{ GeV}$. One of the most striking discoveries at HERA was the observation of the strong rise of the gluon density at small values of Bjorken x . HERA provided the measurement of the parton densities with high accuracy, necessary for precise theoretical calculations of a vast range of processes under study at the Large Hadron Collider. Another discovery of HERA was the observation of a large ($\sim 10\%$) fraction of diffractive events in DIS [1, 2], see the review [3] and refs. therein. In these events the proton stays intact or dissociates into a state with the proton quantum numbers, despite undergoing a violent, highly energetic collision, and is separated from the rest of the produced particles by a large rapidity gap. In a series of ground-breaking papers, the HERA experiments

determined the deep inelastic structure of the t -channel exchange in these events in the form of diffractive parton densities.

Future DIS machines could explore this phenomenon at higher energies and with much higher precision. The Large Hadron-electron Collider (LHeC) is a proposal [4–6] for an ep and eA machine at CERN. It would utilize the 7 TeV proton beam from the LHC and collide it with a 60 GeV electron beam accelerated by an energy recovery linac, thus reaching a centre-of-mass energy $\sqrt{s} = 1.3$ TeV. Dedicated studies of the machine parameters [7, 8] show that its peak luminosity would reach $10^{34} \text{ cm}^{-2} \text{ s}^{-1}$, about three orders of magnitude higher than HERA. The projected running of the machine is over three periods. In the initial run period the total integrated luminosity is estimated to be 50 fb^{-1} . Throughout the entire operation the LHeC is projected to reach 1 ab^{-1} integrated luminosity. It would also be the first electron–nucleus collider, as it would scatter electrons on a beam of nuclei from the LHC, with an energy of 2.75 TeV per nucleon resulting in the centre-of-mass energy per nucleon $\sqrt{s} = 812$ GeV. The integrated luminosity for collisions on nuclei is projected to be of the order 10 fb^{-1} which is ten times larger than the total luminosity collected in ep at HERA. This would allow measurements of nuclear structure with unprecedented precision. Beyond LHeC, the next generation ep collider would be the Future Circular Collider in electron-hadron mode (FCC-eh), utilizing the 50 TeV proton beam from the FCC [9, 10] which would probe DIS at centre-of-mass energy of $\sqrt{s} = 3.5$ TeV with a total integrated luminosity of several ab^{-1} . The eA collisions at the FCC-eh [7, 8] would be performed with a lead beam with energy per nucleon $\sqrt{s} = 19.7$ TeV which would give a centre-of-mass energy per nucleon of $\sqrt{s} = 2.2$ TeV.

These machines would facilitate the study the proton and nuclear structure with extremely high precision. They would unravel complete details of the partonic structure of the proton, explore novel QCD dynamics at small values of Bjorken x , constrain the Higgs properties, perform searches for physics beyond the Standard Model, and provide complementary precision measurements of electroweak physics to e^+e^- colliders and the LHC. DIS on nuclei would allow the study of nuclear structure in a previously unexplored kinematic region in (x, Q^2) . It is therefore expected to thoroughly transform our present knowledge on parton structure in nuclei, also largely strengthening the chromodynamic base for the Quark Gluon Plasma and the ridge correlation phenomenon.

In this work we perform a thorough analysis of the capability of the LHeC and FCC-eh machines to explore inclusive diffraction in DIS. We first determine the accessible kinematic range for diffraction of both machines. Using a very conservative assumption of 2 fb^{-1} for the integrated luminosity we perform a simulation of the data for inclusive coherent ep diffraction in the projected parameter space. This is performed by extending the fits used to extract the diffractive parton densities (DPDFs) at HERA. We then demonstrate the potential of both machines to constrain the DPDFs and point out the sensitivity to the interesting region of low Q^2 where higher twist effects are expected to play an important role. These machines would also be able to explore the top quark contribution to diffraction as well as measuring diffraction in the charged current exchange, though we do not perform analysis of these interesting phenomena here. We also perform a simulation of the diffractive pseudodata for eA collisions for different scenarios of nuclear shadowing. Nuclear diffractive parton distributions have never been measured and therefore the considered machines would be the first to extract these important quantities. It would also be possible to investigate the relation between nuclear shadowing and diffraction.

The structure of the paper is the following. In Sec. 2 we recall the formulae for the diffractive cross sections, the factorization of the inclusive diffractive structure functions and the origin of their sensitivity to DPDFs. In Sec. 3 we present the details of the simulations for the diffractive

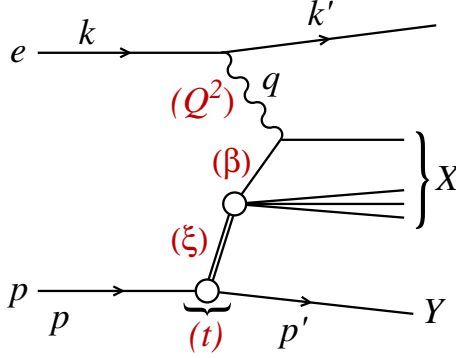


Figure 1: A diagram of a diffractive NC event in DIS together with the corresponding variables, in the one-photon exchange approximation. The large rapidity gap is between the system X and the scattered proton Y (or its low mass excitation).

DIS. In particular, in subsection 3.1 we discuss the parametrization used at HERA, in 3.2 we show the details of the diffractive kinematic range in new machines, and in 3.3 the method to obtain the projected pseudodata with errors is discussed. In Sec. 4 we present our fitting methodology and the potential for constraining the diffractive parton densities by both machines. Sec. 5 is devoted to the prospects of the diffractive deep inelastic in nuclei. Finally we summarize our findings in Sec. 6.

2 Diffractive cross section and diffractive PDFs

In Fig. 1 we show a diagram depicting a neutral current diffractive deep inelastic event. Charged currents could also be considered and they were measured at HERA [11] but with large statistical uncertainties and in a very restricted region of phase space. Although they could be measured at both the LHeC and the FCC-eh with larger statistics and more extended kinematics, in this first study we limit ourselves to neutral currents. The incoming electron or positron, with four momentum k , scatters off the proton, with incoming momentum p , and the interaction proceeds through the exchange of a virtual photon with four-momentum q . The kinematic variables for such an event include the standard deep inelastic variables

$$Q^2 = -q^2, \quad x = \frac{-q^2}{2p \cdot q}, \quad y = \frac{p \cdot q}{p \cdot k}, \quad (1)$$

where Q^2 describes the photon virtuality, x is the Bjorken variable and y the inelasticity of the process. In addition, the variables

$$s = (k + p)^2, \quad W^2 = (q + p)^2, \quad (2)$$

are the electron-proton centre-of-mass energy squared and the photon-proton centre-of-mass energy squared, respectively. The distinguishing feature of the diffractive event $ep \rightarrow eXY$ is the presence of the large rapidity gap between the diffractive system, characterized by the invariant mass M_X and the final proton (or its low-mass excitation) Y with four momentum p' . In addition to the standard DIS variables listed above, diffractive events are also characterized

by an additional set of variables defined as

$$t = (p - p')^2, \quad \xi = \frac{Q^2 + M_X^2 - t}{Q^2 + W^2}, \quad \beta = \frac{Q^2}{Q^2 + M_X^2 - t}. \quad (3)$$

In the above t is the squared four-momentum transfer at the proton vertex, ξ (alternatively denoted by x_P) can be interpreted as the momentum fraction of the ‘diffractive exchange’ with respect to the hadron, and β is the momentum fraction of the parton with respect to the diffractive exchange. The two momentum fractions combine to give Bjorken- x , $x = \beta\xi$.

The physical picture suggested by Fig. 1 is that the initial proton splits into a final state Y of momentum $p' \simeq (1 - \xi)p$ and the object which is responsible for the diffractive exchange of momentum ξp . The latter in turn undergoes a DIS-like process to produce the final state X (see Sec. 3.1 for more details). The study presented in this paper concerns coherent diffraction (i.e. the non-dissociating case), where the final state Y is a proton. Experimentally, this requires tagging of the final proton, which was performed at HERA using Roman pot insertions to the forward beam-pipe, for example the FPS (LPS) of the H1 (ZEUS) collaborations. Most of the HERA data are based, however, on the large rapidity gap (LRG) technique, which results in a small proton dissociative admixture – the response from detector components at very forward rapidities, supplemented with dedicated MC modelling, were used to normalize these results to the coherent cross-sections [11, 12].

Diffractive cross sections in the neutral current case can be presented in the form of the reduced cross sections [11]

$$\frac{d^4\sigma^D}{d\xi d\beta dQ^2 dt} = \frac{2\pi\alpha_{\text{em}}^2}{\beta Q^4} Y_+ \sigma_r^{\text{D}(4)}, \quad (4a)$$

or, upon integration over t ,

$$\frac{d^3\sigma^D}{d\xi d\beta dQ^2} = \frac{2\pi\alpha_{\text{em}}^2}{\beta Q^4} Y_+ \sigma_r^{\text{D}(3)}, \quad (4b)$$

where $Y_+ = 1 + (1 - y)^2$ and the reduced cross sections can be expressed in terms of two diffractive structure functions F_2^D and F_L^D . In the one-photon approximation, the relations are

$$\sigma_r^{\text{D}(3)} = F_2^{\text{D}(3)}(\beta, \xi, Q^2) - \frac{y^2}{Y_+} F_L^{\text{D}(3)}(\beta, \xi, Q^2), \quad (5a)$$

$$\sigma_r^{\text{D}(4)} = F_2^{\text{D}(4)}(\beta, \xi, Q^2, t) - \frac{y^2}{Y_+} F_L^{\text{D}(4)}(\beta, \xi, Q^2, t). \quad (5b)$$

Note that the structure functions $F_{2,L}^{\text{D}(4)}$ have dimension GeV^{-2} , while $F_{2,L}^{\text{D}(3)}$ are dimensionless. In this analysis we neglect Z^0 exchange, though it should be included in future studies.

The reduced cross sections σ_r^D depend on centre-of-mass energy via $y = \frac{Q^2}{\xi\beta s}$. The Y_+ factors ensure that in the region where y is not too close to unity,

$$\sigma_r^D \simeq F_2^D \quad (6)$$

to good approximation.

Both $\sigma_r^{\text{D}(3)}$ and $\sigma_r^{\text{D}(4)}$ have been measured at the HERA collider [1, 2, 11–17] and used to obtain QCD-inspired parametrizations.

The standard perturbative QCD approach to diffractive cross sections is based on collinear factorization [18–20]. It was demonstrated that, similarly to the inclusive DIS cross section, the diffractive cross section can be written, up to terms of order $\mathcal{O}(1/Q^2)$, in a factorized form

$$d\sigma^{ep \rightarrow eXY}(\beta, \xi, Q^2, t) = \sum_i \int_{\beta}^1 dz d\hat{\sigma}^{ei}\left(\frac{\beta}{z}, Q^2\right) f_i^D(z, \xi, Q^2, t), \quad (7)$$

where the sum is performed over all parton flavours (gluon, d -quark, u -quark, etc.). The hard scattering partonic cross section $d\hat{\sigma}^{ei}$ can be computed perturbatively in QCD and is the same as in the inclusive deep inelastic scattering case. The long distance part f_i^D corresponds to the diffractive parton distribution functions, which can be interpreted as conditional probabilities for partons in the proton, provided the proton is scattered into the final state system Y with specified 4-momentum p' . They are evolved using the DGLAP evolution equations [21–24] similarly to the inclusive case. The analogous formula for the t -integrated structure functions reads

$$F_{2/L}^{D(3)}(\beta, \xi, Q^2) = \sum_i \int_{\beta}^1 \frac{dz}{z} C_{2/L,i}\left(\frac{\beta}{z}\right) f_i^{D(3)}(z, \xi, Q^2), \quad (8)$$

where the coefficient functions $C_{2/L,i}$ are same as in inclusive DIS.

3 Simulations for the electron-proton DIS

3.1 Diffractive PDF parametrizations and HERA data

Fits to the diffractive structure functions were performed by H1 [11] and ZEUS [15]. They both parameterize the diffractive PDFs in a two component model, which is a sum of two exchange contributions, \mathbb{P} and \mathbb{R} :

$$f_i^{D(4)}(z, \xi, Q^2, t) = f_{\mathbb{P}}^p(\xi, t) f_i^{\mathbb{P}}(z, Q^2) + f_{\mathbb{R}}^p(\xi, t) f_i^{\mathbb{R}}(z, Q^2). \quad (9)$$

For both of these terms vertex factorization is assumed, meaning that the diffractive exchange can be interpreted as colourless objects called a ‘Pomeron’ or a ‘Reggeon’ with parton distributions $f_i^{\mathbb{P},\mathbb{R}}(\beta, Q^2)$. The flux factors $f_{\mathbb{P},\mathbb{R}}^p(\xi, t)$ represent the probability that a Pomeron/Reggeon with given values ξ, t couples to the proton. They are parametrized using the form motivated by Regge theory

$$f_{\mathbb{P},\mathbb{R}}^p(\xi, t) = A_{\mathbb{P},\mathbb{R}} \frac{e^{B_{\mathbb{P},\mathbb{R}} t}}{\xi^{2\alpha_{\mathbb{P},\mathbb{R}}(t)-1}}, \quad (10)$$

with a linear trajectory $\alpha_{\mathbb{P},\mathbb{R}}(t) = \alpha_{\mathbb{P},\mathbb{R}}(0) + \alpha'_{\mathbb{P},\mathbb{R}} t$. The diffractive PDFs relevant to the t -integrated cross-sections read

$$f_i^{D(3)}(z, \xi, Q^2) = \phi_{\mathbb{P}}^p(\xi) f_i^{\mathbb{P}}(z, Q^2) + \phi_{\mathbb{R}}^p(\xi) f_i^{\mathbb{R}}(z, Q^2), \quad (11)$$

with

$$\phi_{\mathbb{P},\mathbb{R}}^p(\xi) = \int dt f_{\mathbb{P},\mathbb{R}}^p(\xi, t). \quad (12)$$

Note that, the notions of ‘Pomeron’ and ‘Reggeon’ used here to model hard diffraction in DIS are, in principle, different from those describing the soft hadron-hadron interactions; in particular, the parameters of the fluxes may be different.

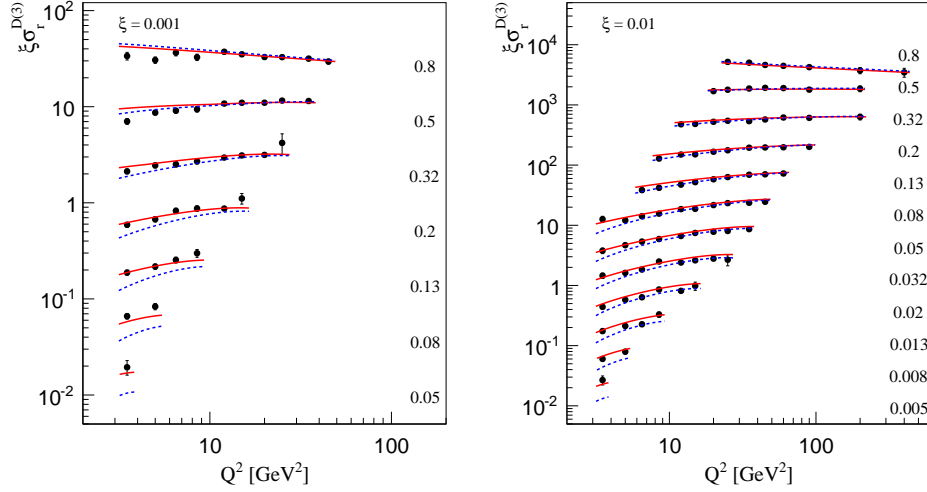


Figure 2: Experimental data from the H1 collaboration at HERA [17] on the reduced diffractive cross section as a function of Q^2 in bins of β for two values of $\xi = 0.001$ (left) and $\xi = 0.01$ (right). The lines indicate predictions from two fits to older data: H1 2006 Fit B (dotted, blue) and ZEUS-SJ (solid, red). The values shown are scaled by 3^k for $k = 0, 1, \dots$ upwards.

The diffractive parton distributions of the Pomeron at the initial scale $\mu_0^2 = 1.8 \text{ GeV}^2$ are parametrized as

$$z f_i^P(z, \mu_0^2) = A_i z^{B_i} (1 - z)^{C_i}, \quad (13)$$

where i is a gluon or a light quark. In the diffractive parametrizations all the light quarks (anti-quarks) are assumed to be equal. For the treatment of heavy flavours, a variable flavour number scheme (VFNS) is adopted, where the charm and bottom quark DPDFs are generated radiatively via DGLAP evolution, and no intrinsic heavy quark distributions are assumed. The structure functions are calculated in a General-Mass Variable Flavour Number scheme (GM-VFNS) [25, 26] which ensures a smooth transition of $F_{2,L}$ across the flavour thresholds by including $\mathcal{O}(m_h^2/Q^2)$ corrections. The parton distributions for the Reggeon component are taken from a parametrization which was obtained from fits to the pion structure function [27, 28].

In Eq. (9) the normalization factors of fluxes, $A_{P,R}$ and of DPDFs, A_i enter in the product. To resolve the ambiguity we fix¹ A_P and use $f_i^R(z, Q^2)$ normalized to the pion structure function, which results in A_i and A_R being well defined free fit parameters.

There are different types of diffractive fits available in the literature. Here we mention the NLO parametrizations from HERA relevant to the current study:

Fit-S: All parameters A_i, B_i, C_i are free, as well as A_R and $\alpha_{P,R}(0)$ (9 parameters). This is the ZEUS-S fit.

Fit-C: Parameters B_g, C_g are set to zero, resulting in a constant gluon density at the starting scale for QCD evolution. This corresponds to the ‘H1 Fit B’ fit when A_R and $\alpha_P(0)$ are free (6 parameters), and to the ZEUS-C fit when A_R and $\alpha_{P,R}(0)$ are free (7 parameters).

Fit-SJ: All parameters A_i, B_i, C_i are free. In addition, dijet production data are used to constrain the gluon. This amounts to the ZEUS-SJ fit when A_R and $\alpha_{P,R}(0)$ are free (9

¹Here, as in the HERA fits, A_P is fixed by normalizing $\phi_P^p(0.003) = 1$.

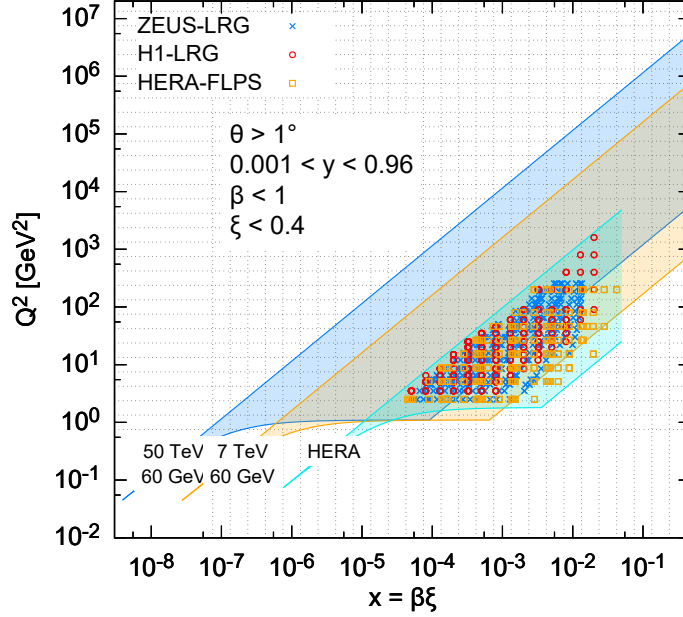


Figure 3: Kinematic phase space for inclusive diffraction in (x, Q^2) for the LHeC (orange region) and the FCC-eh (blue region) as compared with the HERA data (ZEUS-LRG [12], H1-LRG [17], HERA-FLPS [30]). The acceptance limit for the electron in the detector design has been assumed to be 1° .

parameters) and to the H1-2007 fit [29] when A_R and $\alpha_P(0)$ are free (8 parameters).

In the current work the ZEUS-SJ parametrization is used for data simulation while the analysis is performed using the Fit-S model.

In Fig. 2 we show example late HERA data [17] compared with two fits, H1 Fit B and ZEUS-SJ. Note that the fits were performed to older data than shown in the Figure.

3.2 LHeC and FCC-eh kinematics compared with HERA data

The kinematic range in (β, Q^2, ξ) is restricted by the following cuts:

- $Q^2 \geq 1.8 \text{ GeV}^2$: due to the fact that the initial distribution for the DGLAP evolution is parametrized at $\mu_0^2 = 1.8 \text{ GeV}^2$. The renormalization and factorization scales are taken to be equal to Q^2 .
- $\xi < 0.4$: by physical and experimental limitations. This rather high ξ value is an experimental challenge and physically enters the phase-space region where the Pomeron contribution should become negligible. Within the two-component model of Eq. (9), at high ξ the cross-section is dominated by the secondary Reggeon contribution, which is poorly fixed by the HERA data. We present this high ξ (> 0.1) region for illustrative purpose and for the sake of discussion of the fit results in Sec. 4.

In Fig. 3 the accessible kinematic range in (x, Q^2) is shown for three machines: HERA, LHeC and FCC-eh. For the LHeC design the range in x is increased by a factor ~ 20 over HERA and the maximum available Q^2 by a factor ~ 100 . The FCC-eh machine would further increase this range with respect to LHeC by roughly one order of magnitude in both x and Q^2 .

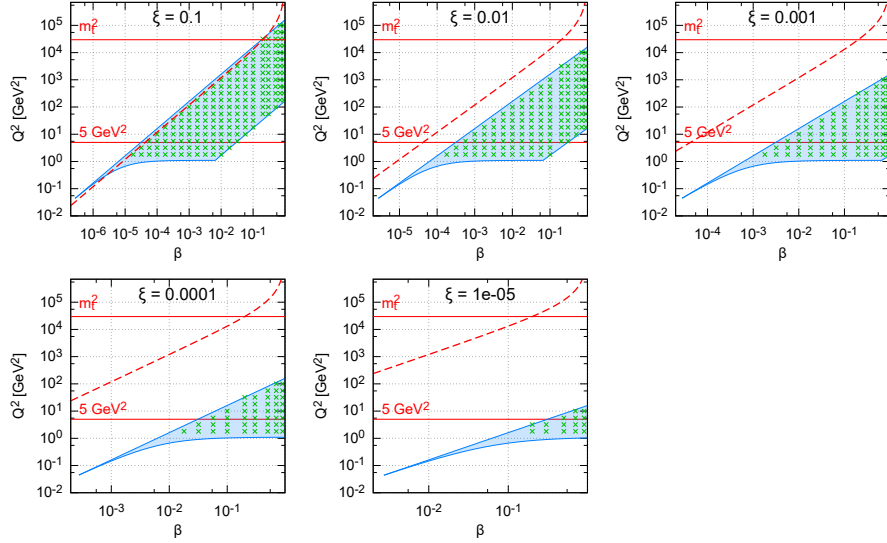


Figure 4: Kinematic phase space for inclusive diffraction in (β, Q^2) for fixed values of ξ for the LHeC design. The horizontal lines indicate correspondingly, $Q^2 = 5 \text{ GeV}^2$, the lowest data value for the DGLAP fit performed in this study and m_t^2 the 6-flavour threshold. The dashed line marks the kinematic limit for $t\bar{t}$ production.

In Fig. 4 and Fig. 5 the phase space in (β, Q^2) is shown for fixed ξ for the LHeC and FCC-eh, respectively. Both machines probe very small values of ξ , the LHeC reaching 10^{-4} with a wide range of β and the FCC-eh extending ξ down to 10^{-5} . Of course, the range in β and ξ is correlated since $x = \beta\xi$. Therefore for small values of ξ only large values of β are accessible while for large ξ the range in β extends to very small values. Above the solid, horizontal line labeled m_t^2 the top quark DPDF comes into play, and above the dashed line the $t\bar{t}$ production channel opens.

3.3 Pseudodata for diffractive structure functions

The reduced cross sections are extrapolated using Eqs.(5a) and (8) with the ZEUS-SJ DPDFs. Following the scenario of the ZEUS fit [15] we work within the VFNS scheme at NLO accuracy. The transition scales for DGLAP evolution are fixed by the heavy quark masses, $\mu^2 = m_h^2$ and the structure functions are calculated in the Thorne–Roberts GM-VFNS [31]. The Reggeon PDFs are taken from the GRV pion set [28], the numerical parameters are taken from Tables 1 and 3 of Ref. [15] and heavy quark masses are $m_c = 1.35 \text{ GeV}$, $m_b = 4.3 \text{ GeV}$.

The model has a non-negligible Reggeon contribution which is hard to constrain from HERA data. It increases with increasing ξ and gives a substantial contribution in the region $\xi > 0.01$ for both the LHeC and the FCC-eh kinematics. Thus it is a source of a large uncertainty on the predictions in this region.

The HERA kinematics give no access to the top quark region, and thus the model provides no reliable contributions from the top quarks. In the following simulations, the top quark contribution to the cross section is neglected, so that the extrapolated cross sections are likely underestimated for $Q^2 > m_t^2$ and $M_X > 2m_t$ – the significance of the top region is discussed in Sec. 4.

The data were generated as the extrapolation of the fit to HERA, amended with a random

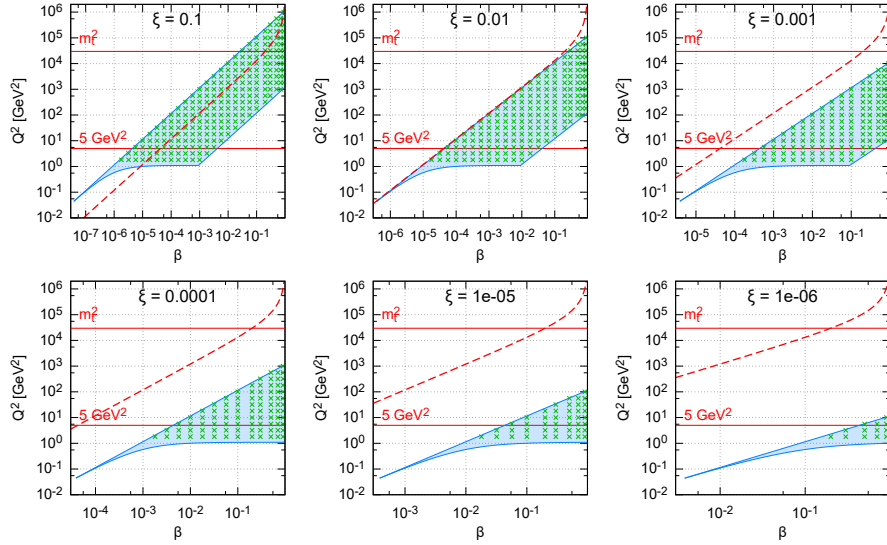


Figure 5: Kinematic phase space for inclusive diffraction in (β, Q^2) for fixed values of ξ for the FCC-eh design. The horizontal lines indicate correspondingly, $Q^2 = 5 \text{ GeV}^2$, the lowest data value for the DGLAP fit performed in this study and m_t^2 the 6-flavour threshold. The dashed line marks the kinematic limit for $t\bar{t}$ production.

Gaussian smearing with standard deviation corresponding to the relative error δ . An uncorrelated 5% systematic error was assumed giving a total error

$$\delta = \sqrt{\delta_{\text{sys}}^2 + \delta_{\text{stat}}^2}. \quad (14)$$

The statistical error was computed assuming a very modest integrated luminosity 2 fb^{-1} , see [7, 8]. For the binning adopted in this study, the statistical uncertainties have a very small effect on the uncertainties in the extracted DPDFs. Obviously, a much larger luminosity would allow a denser binning that would result in smaller DPDF uncertainties.

In Fig. 6 and Fig. 7 we show a subset of the simulated data for the diffractive reduced cross section $\xi\sigma_{\text{red}}$ as a function of β in selected bins of ξ and Q^2 for the LHeC and FCC-eh cases, respectively. For the most part the errors are very small, and are dominated by the systematics. The breaking of Regge factorisation evident at large ξ comes from the large Reggeon contribution in that region, whose validity could be further investigated at the LHeC and FCC-eh.

4 Potential for constraining diffractive PDFs at the LHeC and FCC-eh

4.1 Fitting methodology and results

To evaluate the precision with which the DPDFs can be determined, several pseudodata sets, corresponding to independent random error samples, were generated. Each pseudodata set was fitted to the reduced cross-sections defined by Eqs. (5a) and (8) in the DPDF model of Sec. 3.1.

The minimal value of Q^2 for the data considered in the fits was set to $Q_{\text{min}}^2 = 5 \text{ GeV}^2$. The reason for this cut-off is to restrict the analysis to the range in which the twist-2 contributions should be dominant. It is expected that if there are any higher twist effects, for example due

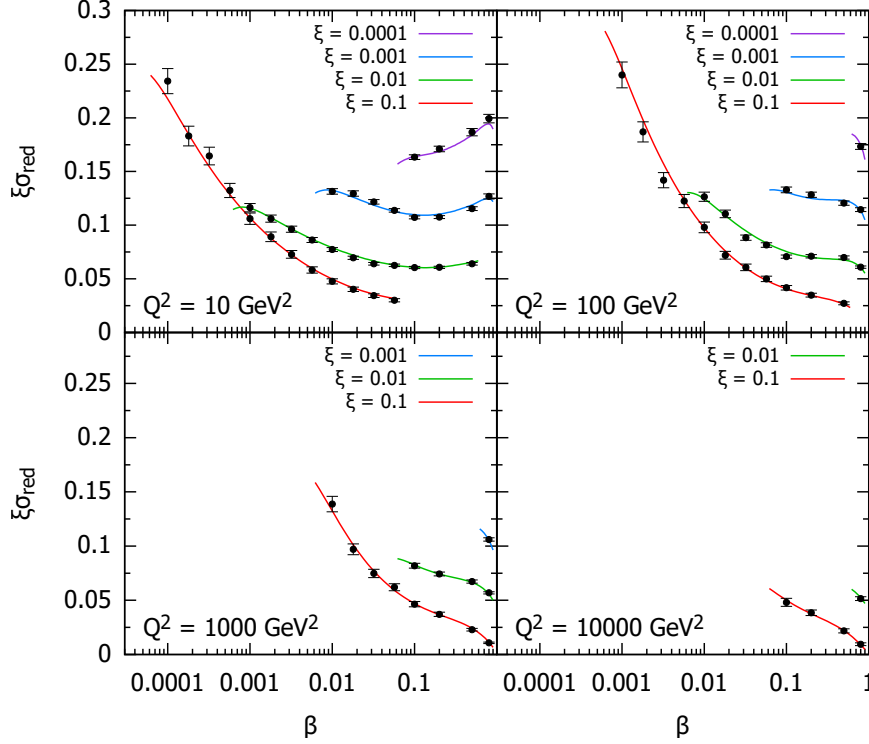


Figure 6: Selected subset of the simulated data for the diffractive reduced cross section as a function of β in bins of ξ and Q^2 for ep collisions at the LHeC.

to parton saturation, they should become visible in the lower Q^2 region. DGLAP fits to the diffractive data are known to not describe the data very well in this region, which may point to the importance of the higher order or higher twist corrections. At HERA, the Q_{\min}^2 values giving acceptable DGLAP (twist-2) fits were 8 GeV² [11] and 5 GeV² [12] for H1 and ZEUS, respectively. Phenomenological studies which include higher twist corrections do indeed describe the HERA data in this region better than the pure DGLAP evolution [32].

The maximum value of ξ was set by default to $\xi_{\max} = 0.1$, above which the cross-section starts to be dominated by the Reggeon exchange. The effects of relaxing both limits Q_{\min}^2 and ξ_{\max} are described below. The region above the top threshold was not considered in the fits. This point however should be addressed in future studies; the top contribution has a negligible impact for the LHeC but some impact for the FCC-eh.

The binning adopted in this study corresponds roughly to 4 bins per order of magnitude in each of ξ, β, Q^2 . For $Q_{\min}^2 = 5$ GeV², $\xi_{\max} = 0.1$ and below the top threshold this results in 1229 and 1735 pseudodata points for the LHeC and FCC-eh, respectively. The top-quark region adds 17 points for the LHeC and 255 for FCC-eh. Lowering Q_{\min}^2 down to 1.8 GeV² we get 1589 and 2171 pseudodata points, while increasing ξ up to 0.32 adds ca. 180 points for both machines.

The potential for determination of the gluon DPDF was investigated by fitting the inclusive diffractive DIS pseudodata with two models, S and C of Sec. 3.1 with $\alpha_{P,R}(0)$ fixed, in order to focus on the shape of the Pomeron's PDFs. At HERA, both S and C fits provide equally good descriptions of the data with $\chi^2/\text{ndf} = 1.19$ and 1.18, respectively, despite different gluon DPDF shapes. The LHeC pseudodata are much more sensitive to gluons, resulting in χ^2/ndf values of 1.05 and 1.4 for the S and C fits, respectively. This motivates the use of the larger

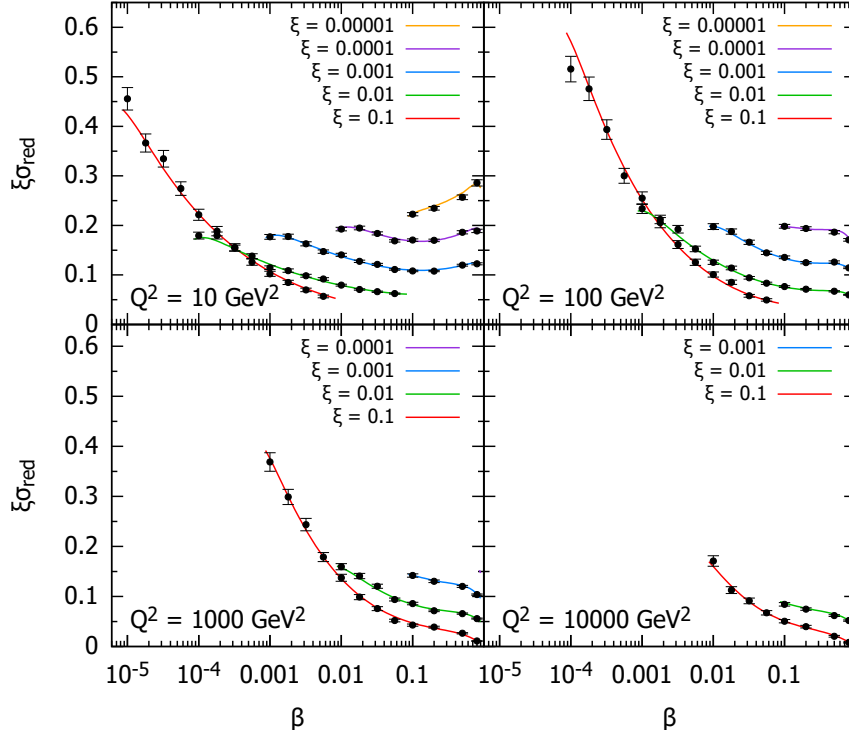


Figure 7: Selected subset of the simulated data for the diffractive reduced cross section as a function of β in bins of ξ and Q^2 for ep collisions at the FCC-eh.

number of parameters in the fit-S model, which we employ in the further studies.

4.2 DPDFs uncertainties

In Fig. 8 and Fig. 9 the diffractive gluon and quark distributions are shown for the LHeC and FCC-eh, respectively, as a function of z for fixed scales $\mu^2 = 6, 20, 60, 200 \text{ GeV}^2$. The bands labelled A, B, C denote fits to three statistically independent pseudodata replicas, obtained from the same central values and statistic and systematic uncertainties. Hereafter the bands shown correspond to $\Delta\chi^2 = 2.7$ uncertainty (90% CL). Also the extrapolated ZEUS-SJ DPDFs are shown with error bands marked by the ‘/’ hatched area. The extrapolation beyond the reach of LHeC/FCC-eh is marked in grey and the HERA kinematic limit is marked with the vertical dotted line. The stability of the results with respect to the replica used for the analysis is evident, so in the following only one will be employed. The DPDFs determination accuracy improves with respect to HERA by a factor of 5–7 for the LHeC and 10–15 for the FCC-eh.

For a better illustration of the precision, in Figs. 10, 11 and 12 the relative uncertainties are shown for parton distributions at different scales. In Fig. 10 the upper plots correspond to the LHeC and the lower ones to the FCC-eh scenarios, respectively. The different bands show the variation with the upper cut on the available ξ range, from 0.01 to 0.32. We observe only a modest improvement in the achievable accuracy of the extracted DPDFs with the change of ξ by an order of magnitude from 0.01 to 0.1. An almost negligible effect is observed when further extending the ξ range up to 0.32. This is encouraging, since the measurement for the very large values of ξ is challenging. It reflects the dominance of the secondary Reggeon in this region.

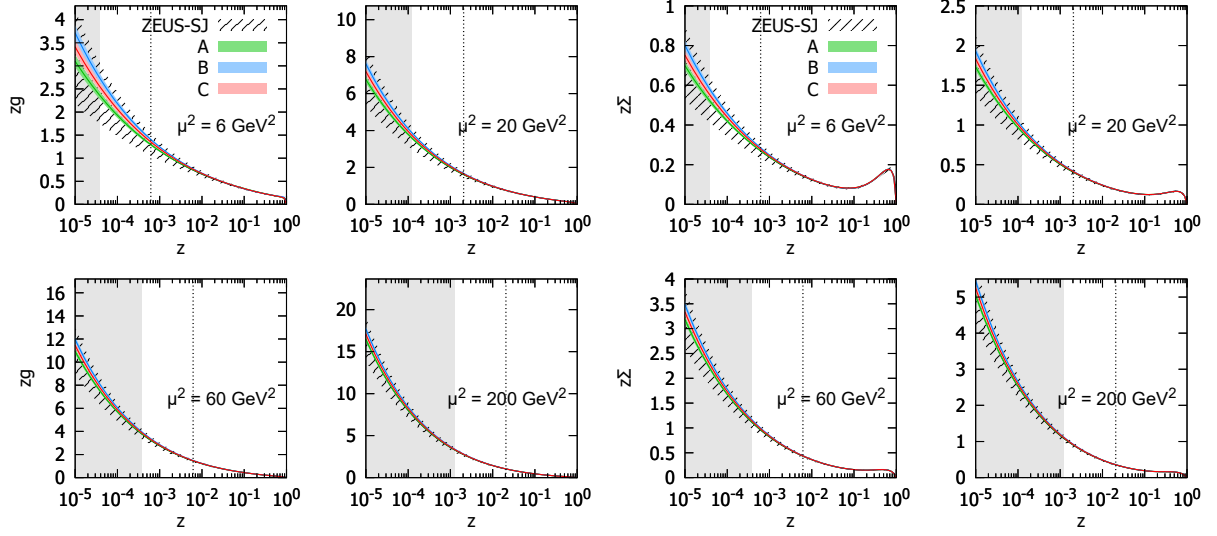


Figure 8: Diffractive PDFs for gluon and quark in the LHeC kinematics as a function of momentum fraction z for fixed values of scale μ^2 . Results of fits to three (A,B,C) pseudodata replicas are shown together with the experimental error bands. For comparison, the extrapolated ZEUS-SJ fit is also shown (black) with error bands marked with the hatched pattern. The vertical dotted lines indicate the HERA kinematic limit.

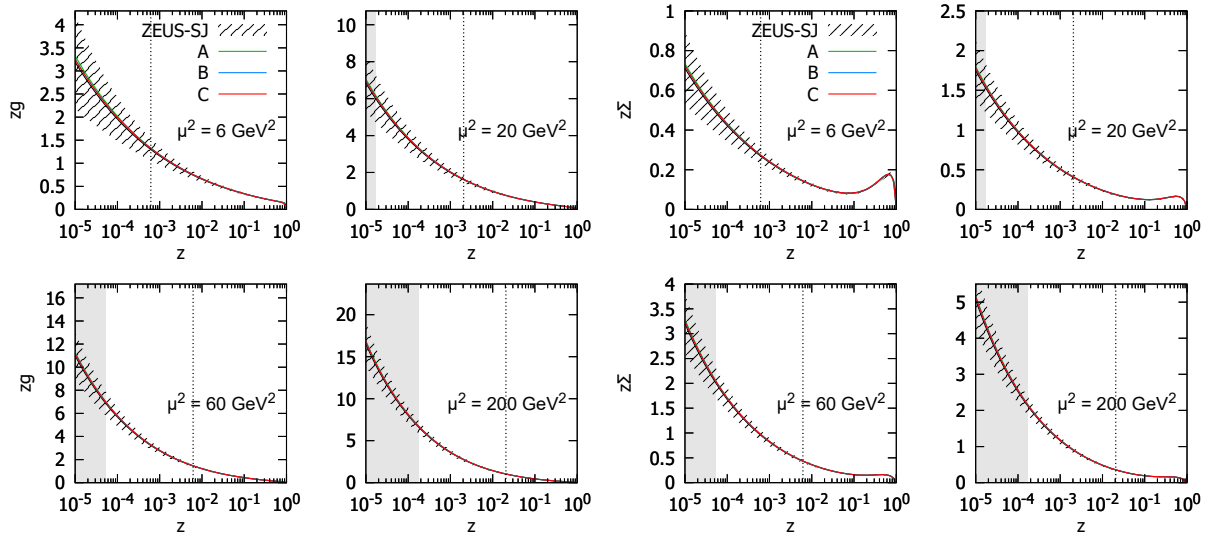


Figure 9: Identical to Fig. 8, but in the FCC-eh kinematics.

In Fig. 11 we show the variation of the relative precision with the change of the minimal value of Q^2 from 1.8 GeV² (curves) to 5 GeV² (bands). The LHeC scenario is indicated in green and FCC-eh in red. There is a quite substantial effect on the achieved precision depending on the minimal value of Q^2 . This is not only related to the fact that the number of pseudodata points is larger by about 300 in each case, but is primarily due to the fact that acceptance across the full range of z in this region is crucial for constraining the initial condition for the

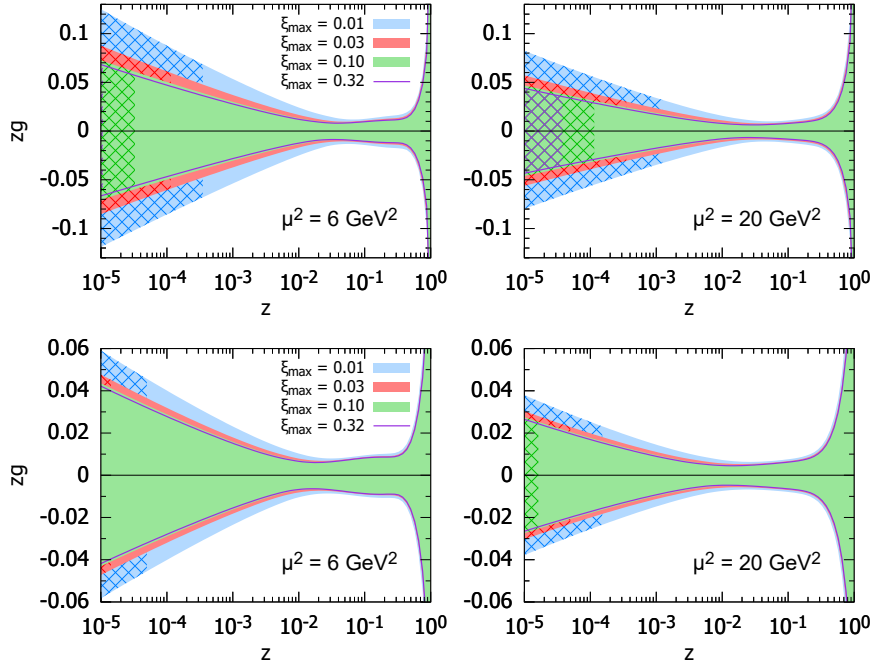


Figure 10: Relative uncertainties on the diffractive gluon PDFs for the LHeC kinematics (upper panel) and FCC-eh kinematics (lower panel). Two different choices of scales are considered $\mu^2 = 6$ and $\mu^2 = 20$ GeV². The blue, red, green bands and magenta line correspond to different maximal values of $\xi = 0.01, 0.03, 0.1, 0.32$, respectively. The cross-hatched areas show kinematically excluded regions.

DGLAP evolution. The more data points are in the region closer to the starting distribution the better it is constrained, particularly at low and medium values of Q^2 and z . Fig. 11 also demonstrates that both machines will be very sensitive to this region and therefore potentially able to constrain higher twists and/or saturation effects.

In Fig. 12 we show the effect on the relative uncertainties for quarks and gluons of making $\alpha_{P,R}(0)$ free fit parameters. The increased number of fitting parameters from 7 to 9 has a very small effect on the DPDF uncertainties. In addition, we note that for low x values the quark and gluon uncertainties are similar, with quark uncertainties being smaller by about 20%. There is, however, a marked difference in the uncertainties for quarks and gluons at large values of z .

5 Diffractive deep inelastic scattering off nuclei

Electron-nucleus (eA) collisions are also possible at the LHeC and the FCC-eh with large integrated luminosities, $\mathcal{L}_{NN} \sim \mathcal{O}(1)$ fb⁻¹, see [4–8]. Similar considerations apply to diffraction in eA as to ep collisions. The main difference is the larger contribution from incoherent diffraction² $e + A \rightarrow e + X + A^*$ than from coherent diffraction $e + A \rightarrow e + X + A$, the former dominating for $|t|$ larger than a few hundredths of a GeV². In the following we focus on coherent diffraction, which could be distinguished from the incoherent case using forward detectors [5].

² A^* denotes a final state in which the nucleus has dissociated to a system of at least two hadrons, but the rapidity gap signature that defines the diffractive event is still present.

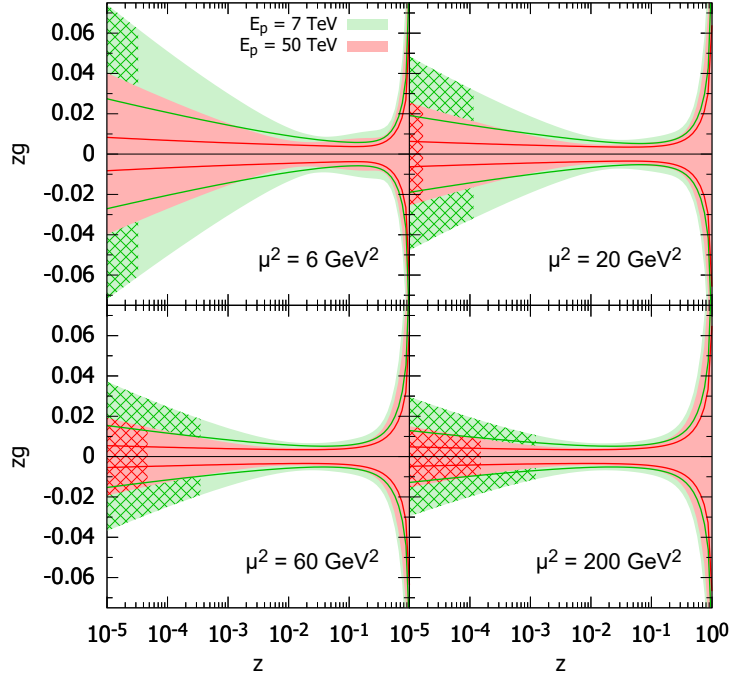


Figure 11: Relative uncertainties on the diffractive gluon PDF extraction for four distinct scales $\mu^2 = 6, 20, 60, 200 \text{ GeV}^2$. The bands correspond to the choice of the high cut-off on the data included in the fit $Q_{\min}^2 = 5 \text{ GeV}^2$ and the lines correspond to the lower choice $Q_{\min}^2 = 1.8 \text{ GeV}^2$. The green colour corresponds to the LHeC scenario and red to the FCC-eh scenario. The cross-hatched areas show kinematically excluded regions.

Assuming the same framework (collinear factorization for hard diffraction, Eq. (7), and Regge factorization, Eq. (9)) described for ep in Sections 2 and 3.1 to hold for eA , nuclear diffractive PDFs (nDPDFs) can be extracted from the diffractive reduced cross sections, Eqs. (4a) and (4b). It should be noted that such nDPDFs have never been measured. With the same electron energy $E_e = 60 \text{ GeV}$ and nuclear beams with $E_N = 2.76$ and 19.7 TeV/nucleon for the LHeC and the FCC-eh, respectively, the kinematic coverage is very similar to that shown in Fig. 3.

Due to the lack of previous measurements, there are no parametrizations for nDPDFs but models exist for the nuclear effects on parton densities defined through the nuclear modification factor

$$R_k^A(\beta, \xi, Q^2) = \frac{f_{k/A}^{D(3)}(\beta, \xi, Q^2)}{A f_{k/p}^{D(3)}(\beta, \xi, Q^2)}, \quad (15)$$

with diffractive parton densities in nucleus A , $f_{k/A}^{D(3)}(\beta, \xi, Q^2)$. We use the model proposed in [33], where parametrizations for nuclear modification factors are provided at the scale $Q^2 = 4 \text{ GeV}^2$ (extended in β and ξ to cover the LHeC and FCC-eh kinematic regions³). Then DGLAP evolution is employed to evolve the ZEUS-SJ proton diffractive PDFs multiplied by R_k^A from [33] to obtain the nuclear diffractive PDFs, at any Q^2 . The structure functions and reduced cross sections are then calculated in the same way as in the proton case, and these results are used

³We thank Vadim Guzey for providing them.

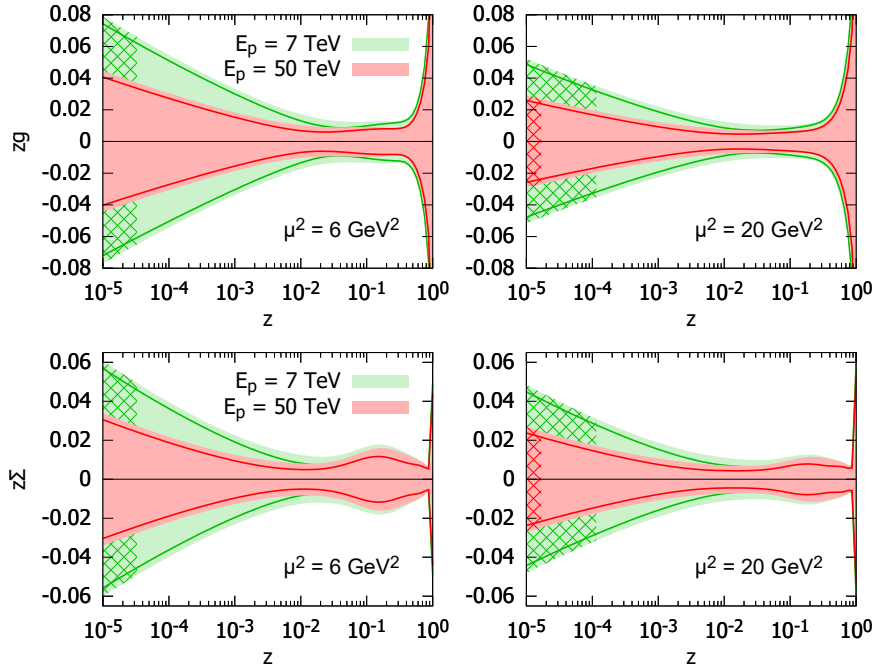


Figure 12: Relative uncertainties on the diffractive PDFs for different numbers of free fit parameters, 7 and 9. Two different choices of scales are considered $\mu^2 = 6$ and 20 GeV^2 . The green and red bands correspond to the 9-parameter fits for the LHeC and FCC-eh scenarios, respectively. The continuous lines delimit the 7-parameter fit uncertainty. The cross-hatched areas show kinematically excluded regions.

to obtain the modification factors, analogous to Eq. (15), for these quantities. We have also repeated the calculation in the Zero-Mass VFNS in order to check that the resulting modification factors do not depend on the applied scheme.

The model in [33] employs Gribov inelastic shadowing [34] which relates diffraction in ep to nuclear shadowing for total and diffractive eA cross sections. It assumes that the nuclear wave function squared can be approximated by the product of one-nucleon densities, neglects the t -dependence of the diffractive γ^* -nucleon amplitude compared to the nuclear form factor, introduces a real part in the amplitudes [35], and considers the colour fluctuation formalism for the inelastic intermediate nucleon states [36]. There are two variants of the model, named H and L, corresponding to different strengths of the colour fluctuations, giving rise to larger and smaller probabilities for diffraction in nuclei with respect to that in proton, respectively. To illustrate the results of this model, in Fig. 13 we show the nuclear modification factor, Eq. (15), for $F_2^{D(3)}$ and $F_L^{D(3)}$ in ^{208}Pb .

Pseudodata were generated using the same method, 5% uncorrelated systematic error and luminosity 2 fb^{-1} as described for ep in Section 3.3. The results for the LHeC and FCC-eh are shown in Figs. 14 and 15, respectively (for a selected subset of bins). The similarly large coverage and small uncertainty (dominated by the assumed systematics) illustrated in these two figures compared to Figs. 6 and 7 makes it clear that an accurate extraction of nDPDFs in ^{208}Pb in an extended kinematic region, similar to that shown in Figs. 8, 9 and 10, will be possible.

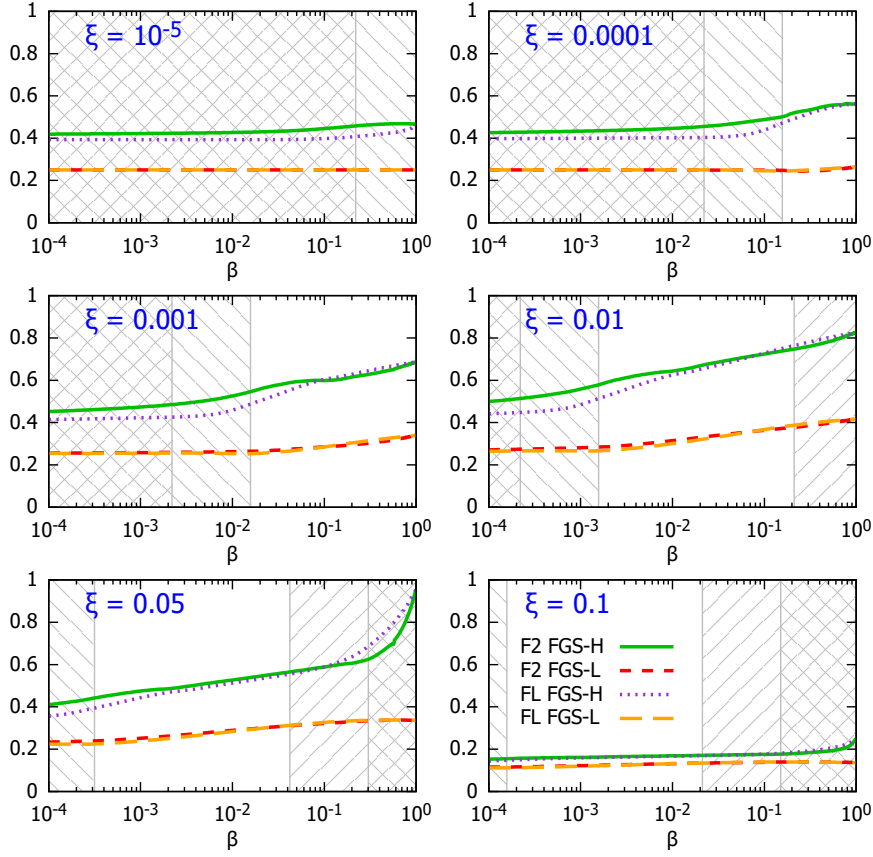


Figure 13: Nuclear modification factor, Eq. (15), for $F_2^{D(3)}$ and $F_L^{D(3)}$ in ^{208}Pb versus β , at $Q^2 = 10 \text{ GeV}^2$ and for different ξ , for the models H and L in [33]. The ‘\’ and ‘/’ hatched areas show kinematically excluded regions for $E = 2.76$ and 19.7 TeV/nucleon , respectively.

6 Conclusions

In this paper we have investigated the potential of the LHeC and FCC-eh machines for the measurement of diffractive cross sections and to constrain the diffractive parton densities. The LHeC machine would extend the available kinematic range in x by a factor of order 20 and the maximum Q^2 by a factor of order 100. The FCC-eh machine would extend the accessible region by an order of magnitude with respect to LHeC both in x and Q^2 . This translates into a range of available ξ down to 10^{-4} at the LHeC and down to 10^{-5} for FCC-eh for a wide range of β . With the assumed very conservative integrated luminosity of 2 fb^{-1} we have generated large pseudodata sets of 1200 – 1800 points for the LHeC and of 1700 – 2600 points for the FCC-eh, depending on the minimum Q^2 . The simulated data have very small error bars, dominated by the assumed 5% systematic error. We have performed fits of the diffractive parton densities to the simulated pseudodata, following the methodology employed previously at HERA. The DPDF determination using the pseudodata substantially improves the precision achieved in the HERA analysis, reducing the DPDF uncertainties by a factor 5 – 7 for the LHeC and 10 – 15 for the FCC-eh. If the luminosity were increased one could perform a finer binning and constrain the extracted DPDFs even more.

The accuracy of the DPDF extraction depends only mildly on the maximal value of ξ . In

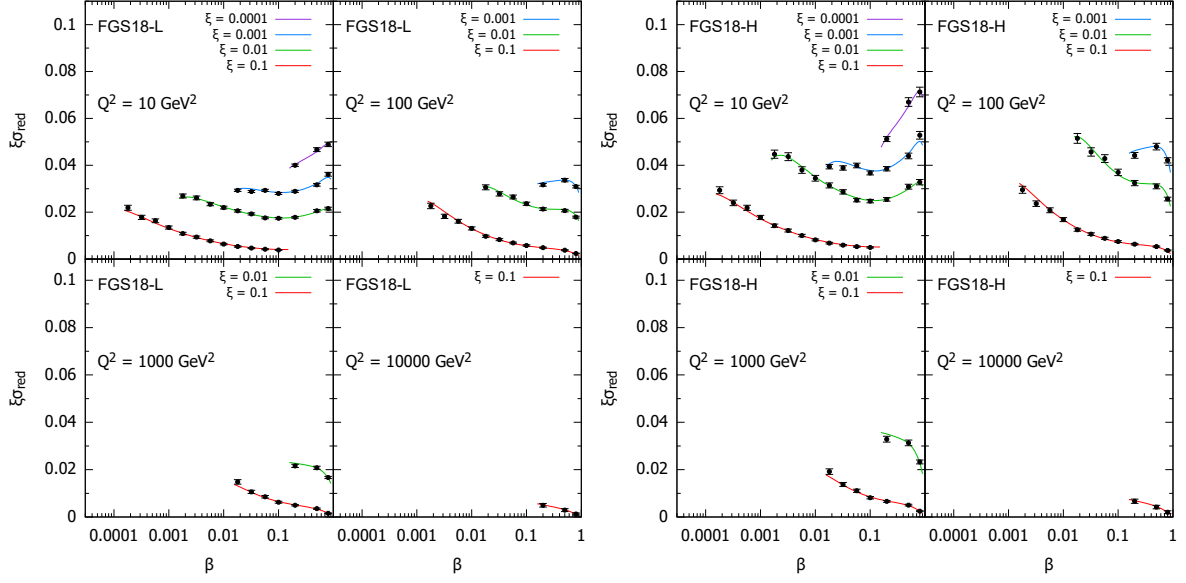


Figure 14: Simulated data for the diffractive reduced cross section as a function of β in bins of ξ and Q^2 for $e^{208}\text{Pb}$ collisions at the LHeC, in the models in [33].

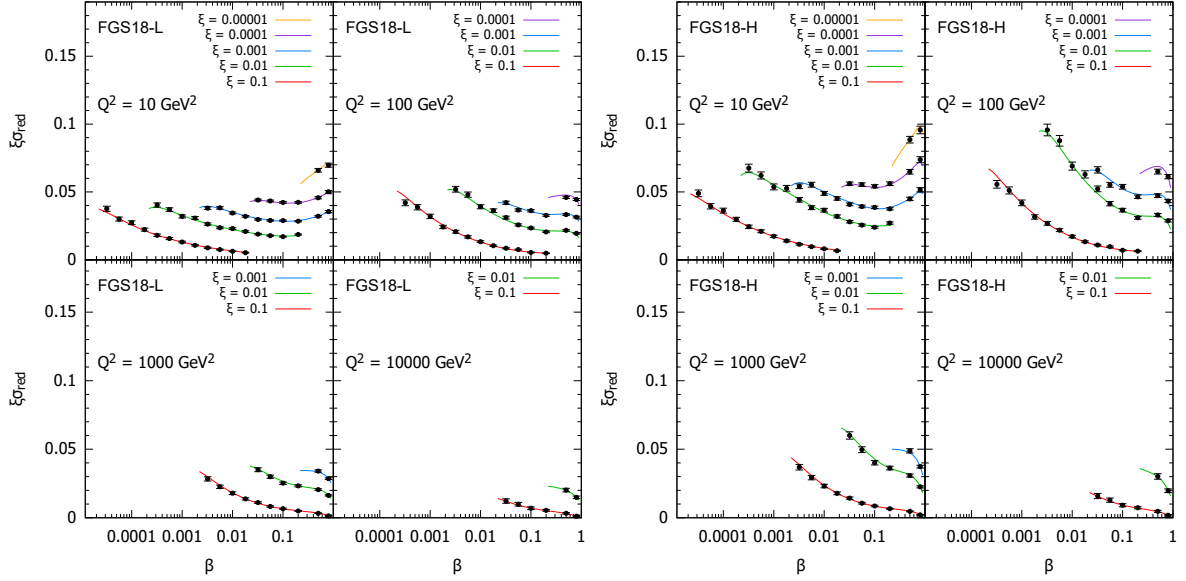


Figure 15: Simulated data for the diffractive reduced cross section as a function of β in bins of ξ and Q^2 for $e^{208}\text{Pb}$ collisions at the FCC-eh, in the models in [33].

particular, we found that changing ξ from 0.32 to 0.1 has a negligible impact on the precision of the extracted DPDFs. This is very encouraging since the large ξ region is very challenging experimentally and theoretically. On the other hand, we found a rather large sensitivity to the functional form of the gluon DPDF; specifically, a flat and non-flat gluon – which were indistinguishable at HERA – produce sizeably different χ^2/ndf at the LHeC and FCC-eh. Besides, the

fits are also sensitive to the assumed minimal value of Q^2 used in the DGLAP fits. This feature is understandable since the DGLAP evolution is very sensitive to the low Q^2 region, which is crucial for constraining the initial condition. This fact indicates the great sensitivity of both machines to physics that goes beyond the standard twist-2 DGLAP evolution. Finally, we have investigated the possibility of inclusive diffraction in the case of nuclear targets. Using models which employ Gribov inelastic shadowing, we make predictions for the nuclear ratios for the diffractive structure functions F_2 and F_L , and provide the simulated data sets. We find that the accurate measurement of the nuclear diffractive cross section would be possible in the nuclear case, with similar coverage in β, ξ and Q^2 and similar precision to the proton case.

The extended kinematic range of both machines offers new exciting possibilities in diffraction. One is that they are sensitive to the top contribution to diffraction. Since HERA did not give access to the top, none of the models used to simulate the pseudodata provides a reliable contribution from the top quark. In the present analysis the top contribution was thus neglected, but it could be investigated in further studies, particularly for the FCC-eh. Furthermore, diffractive dijets could also be included and their impact on the extraction of DPDFs evaluated. Another interesting possibility is that of charged current diffraction. This was measured at HERA but in a very limited kinematic range and with very small statistics. In future DIS machines this would certainly be a much better explored process and would provide additional tests for factorization in diffraction.

Summarizing, both the LHeC and its higher energy version, the FCC-eh, offer unprecedented capabilities for studying diffraction both in ep and eA . This first exploratory study illustrates some of the huge range of opportunities. More extensive studies, both on the phenomenological side and at detector level, are left for the future. These new possibilities for investigating proton and nuclear structure will eventually open new avenues in the understanding of dynamics beyond linear evolution, such as higher twists and non-linear effects, and, ultimately, hopefully, confinement.

Acknowledgments

We thank Vadim Guzey for providing the FGS parametrization and Max Klein for reading the manuscript. We also thank John Collins and Krzysztof Golec-Biernat for discussions. NA was supported by Ministerio de Ciencia e Innovación of Spain under projects FPA2014-58293-C2-1-P, FPA2017-83814-P and Unidad de Excelencia María de Maetzu under project MDM-2016-0692, by Xunta de Galicia (Consellería de Educación) within the Strategic Unit AGRUP2015/11, and by FEDER. This work has been performed in the framework of COST Action CA15213 ‘Theory of hot matter and relativistic heavy-ion collisions’ (THOR). WS was supported by the National Science centre, Poland, Grant No. 2014/13/B/ST2/02486. AMS was supported by the Department of Energy Grant No. DE-SC-0002145, as well as the National Science centre, Poland, Grant No. 2015/17/B/ST2/01838.

References

- [1] C. Adloff et al., “Inclusive measurement of diffractive deep inelastic ep scattering”, *Z. Phys.*, vol. C76, pp. 613–629, 1997.
- [2] J. Breitweg et al., “Measurement of the diffractive structure function $F_2(D(4))$ at HERA”, *Eur. Phys. J.*, vol. C1, pp. 81–96, 1998.

- [3] Paul Newman and Matthew Wing, “The Hadronic Final State at HERA”, *Rev. Mod. Phys.*, vol. 86, no. 3, pp. 1037, 2014.
- [4] J. B. Dainton, M. Klein, P. Newman, E. Perez, and F. Willeke, “Deep inelastic electron-nucleon scattering at the LHC”, *JINST*, vol. 1, pp. P10001, 2006.
- [5] J. L. Abelleira Fernandez et al., “A Large Hadron Electron Collider at CERN: Report on the Physics and Design Concepts for Machine and Detector”, *J. Phys.*, vol. G39, pp. 075001, 2012.
- [6] Max Klein, “Future Deep Inelastic Scattering with the LHeC”, in *From My Vast Repertoire ...: Guido Altarelli’s Legacy*, Aharon Levy, Stefano Forte, and Giovanni Ridolfi, Eds., pp. 303–347, 2019, [arXiv:1802.04317\[hep-ph\]](#).
- [7] Frederick Bordry, Michael Benedikt, Oliver Bruning, John Jowett, Lucio Rossi, Daniel Schulte, Steinar Stapnes, and Frank Zimmermann, “Machine Parameters and Projected Luminosity Performance of Proposed Future Colliders at CERN”, 2018, [arXiv:1810.13022\[physics.acc-ph\]](#).
- [8] Oliver Bruning, John Jowett, Max Klein, Daniel Pellegrini, Daniel Schulte, and Frank Zimmermann, “Future Circular Collider Study FCC-eh Baseline Parameters”, CERN FCC-ACC-RPT-012, 2017.
- [9] Edited by M. Mangano et al., “Future Circular Collider Study. Volume 1: Physics Opportunities. Conceptual Design Report”, CERN-ACC-2018-0056, 2018.
- [10] Edited by M. Benedikt et al., “Future Circular Collider Study. Volume 3: The Hadron Collider (FCC-hh) . Conceptual Design Report”, CERN-ACC-2018-0058, 2018.
- [11] A. Aktas et al., “Measurement and QCD analysis of the diffractive deep-inelastic scattering cross-section at HERA”, *Eur.Phys.J.*, vol. C48, pp. 715–748, 2006.
- [12] S. Chekanov et al., “Deep inelastic scattering with leading protons or large rapidity gaps at HERA”, *Nucl.Phys.*, vol. B816, pp. 1–61, 2009.
- [13] S. Chekanov et al., “Study of deep inelastic inclusive and diffractive scattering with the ZEUS forward plug calorimeter”, *Nucl. Phys.*, vol. B713, no. 1-3, pp. 3–80, 2005.
- [14] A. Aktas et al., “Diffractive deep-inelastic scattering with a leading proton at HERA”, *Eur.Phys.J.*, vol. C48, pp. 749–766, 2006.
- [15] S. Chekanov et al., “A QCD analysis of ZEUS diffractive data”, *Nucl.Phys.*, vol. B831, pp. 1–25, 2010.
- [16] F.D. Aaron et al., “Measurement of the cross section for diffractive deep-inelastic scattering with a leading proton at HERA”, *Eur.Phys.J.*, vol. C71, pp. 1578, 2011.
- [17] F.D. Aaron et al., “Inclusive Measurement of Diffractive Deep-Inelastic Scattering at HERA”, *Eur.Phys.J.*, vol. C72, pp. 2074, 2012.
- [18] John C. Collins, “Proof of factorization for diffractive hard scattering”, *Phys. Rev.*, vol. D57, pp. 3051–3056, 1998, [Erratum: *Phys. Rev.*D61,019902(2000)].

- [19] Arjun Berera and Davison E. Soper, “Behavior of diffractive parton distribution functions”, *Phys. Rev.*, vol. D53, pp. 6162–6179, 1996.
- [20] L. Trentadue and G. Veneziano, “Fracture functions: An Improved description of inclusive hard processes in QCD”, *Phys. Lett.*, vol. B323, pp. 201–211, 1994.
- [21] V. N. Gribov and L. N. Lipatov, “ $e^+ e^-$ pair annihilation and deep inelastic $e p$ scattering in perturbation theory”, *Sov. J. Nucl. Phys.*, vol. 15, pp. 675–684, 1972, [*Yad. Fiz.*15,1218(1972)].
- [22] V. N. Gribov and L. N. Lipatov, “Deep inelastic $e p$ scattering in perturbation theory”, *Sov. J. Nucl. Phys.*, vol. 15, pp. 438–450, 1972, [*Yad. Fiz.*15,781(1972)].
- [23] Guido Altarelli and G. Parisi, “Asymptotic Freedom in Parton Language”, *Nucl. Phys.*, vol. B126, pp. 298–318, 1977.
- [24] Yuri L. Dokshitzer, “Calculation of the Structure Functions for Deep Inelastic Scattering and $e^+ e^-$ Annihilation by Perturbation Theory in Quantum Chromodynamics.”, *Sov. Phys. JETP*, vol. 46, pp. 641–653, 1977, [*Zh. Eksp. Teor. Fiz.*73,1216(1977)].
- [25] John C. Collins and Wu-Ki Tung, “Calculating Heavy Quark Distributions”, *Nucl. Phys.*, vol. B278, pp. 934, 1986.
- [26] R. S. Thorne and W. K. Tung, “PQCD Formulations with Heavy Quark Masses and Global Analysis”, 2008.
- [27] J. F. Owens, “ Q^2 Dependent Parametrizations of Pion Parton Distribution Functions”, *Phys. Rev.*, vol. D30, pp. 943, 1984.
- [28] M. Gluck, E. Reya, and A. Vogt, “Pionic parton distributions”, *Z. Phys.*, vol. C53, pp. 651–656, 1992.
- [29] A. Aktas et al., “Dijet Cross Sections and Parton Densities in Diffractive DIS at HERA”, *JHEP*, vol. 10, pp. 042, 2007.
- [30] F.D. Aaron et al., “Combined inclusive diffractive cross sections measured with forward proton spectrometers in deep inelastic ep scattering at HERA”, *Eur.Phys.J.*, vol. C72, pp. 2175, 2012.
- [31] R. S. Thorne and R. G. Roberts, “An ordered analysis of heavy flavour production in deep inelastic scattering”, *Phys. Rev.*, vol. D57, pp. 6871–6898, 1998.
- [32] L. Motyka, M. Sadzikowski, and W. Slominski, “Evidence of strong higher twist effects in diffractive DIS at HERA at moderate Q^2 ”, *Phys. Rev.*, vol. D86, pp. 111501, 2012.
- [33] L. Frankfurt, V. Guzey, and M. Strikman, “Leading Twist Nuclear Shadowing Phenomena in Hard Processes with Nuclei”, *Phys. Rept.*, vol. 512, pp. 255–393, 2012.
- [34] V. N. Gribov, “Glauber corrections and the interaction between high-energy hadrons and nuclei”, *Sov. Phys. JETP*, vol. 29, pp. 483–487, 1969, [*Zh. Eksp. Teor. Fiz.*56,892(1969)].
- [35] V. N. Gribov and Alexander A. Migdal, “Properties of the pomeron pole and the branch cuts related to it at low momentum transfer”, *Sov. J. Nucl. Phys.*, vol. 8, pp. 583–590, 1969, [*Yad. Fiz.*8,1002(1968)].

- [36] L. L. Frankfurt, G. A. Miller, and M. Strikman, “The Geometrical color optics of coherent high-energy processes”, *Ann. Rev. Nucl. Part. Sci.*, vol. 44, pp. 501–560, 1994.